Development of Gait Measurement Robot for Prevention of Falls in the Elderly

Ayanori Yorozu[1], Mayumi Ozawa[1] and Masaki Takahashi[2]
[1]*School of Science for Open and Environmental Systems, Keio University, 3-14-1 Hiyoshi, Kohoku-ku, Yokohama 223-8522, Japan*
[2]*Department of System Design Engineering, Keio University, 3-14-1 Hiyoshi, Kohoku-ku, Yokohama 223-8522, Japan*

Keywords: Gait Measurement, Omnidirectional Mobile Robot, Kalman Filter, Laser Range Sensor.

Abstract: To prevent falls in the elderly, gait measurements such as several-meters walking test and gait trainings are carried out in community health activities. To evaluate the risk of falling of the participant, it is necessary to measure foot contact times and positions so that the stride length of each leg and the walking speed can be used as evaluation parameters. However, the conventional measurement systems are difficult to install for use in community health activities because of their scale, cost and constraints of the measurement range. In this study, we propose a novel gait measurement system which uses an autonomous mobile robot with laser range sensor (LRS) for a long-distance walking test in a real living space regardless of detection range of sensor. The robot sequentially estimates its own pose and acquires the position of both legs of the participant. The robot leads the participant from the start to the goal of the walking test while maintaining a certain distance from the participant. Then, the foot contact times and the positions are calculated by analyzing estimated position and speed of each leg. From the experimental results, it was confirmed that the proposed robot could acquire the foot contact times and positions.

1 INTRODUCTION

With our society rapidly aging, there is a worry that the burden on families who have members in need of nursing care will increase. Falling is one of the main factors that cause elderly people to require nursing care (WHO, 2008), and one-third of community-dwelling individuals aged over 75 years will experience at least one fall a year (Tinetti, et al., 1988).

To prevent falls in the elderly, gait measurements and trainings are carried out in community health activities. As shown in Figure 1 (a), one of the representative gait measurement to evaluate motor function is a several-meters walking test. In addition, it has been reported that elderly people at high risk of falling decrease a dual-task performance including not only motor function but also cognitive function (Melzer and Oddsson, 2004), (Yamada, et al., 2011). As shown in Figure 1 (b), to enhance not only motor function but also cognitive function, gait trainings where the participant steps on the target square following instructions displayed on a screen have been proposed (Schoene, et al., 2013), (Yamada, et al., 2012). To evaluate the risk of falling of the participant, it is necessary to measure foot contact times and positions so that the stride length of each leg and the walking speed can be used as evaluation parameters.

Generally, force plates (Melze, et al., 2007) or three-dimensional motion analysis devices (Davis, et al., 1991) have been used in gait analysis. However, it is difficult to install these devices for use in

(a) 10 m walking test to evaluate motor function (Kakamigahara, 2007)

(b) Home-based step training to enhance dual-task performance (Schoene, et al., 2013)

Figure 1: Example of gait measurements and trainings in community health activities.

Yorozu A., Ozawa M. and Takahashi M..
Development of Gait Measurement Robot for Prevention of Falls in the Elderly.
DOI: 10.5220/0005058001270135
In *Proceedings of the 11th International Conference on Informatics in Control, Automation and Robotics* (ICINCO-2014), pages 127-135
ISBN: 978-989-758-040-6

community health activities because of their scale and cost. Consequently, measurements during community health activities are often carried out by observation using a stopwatch, making it difficult to measure foot contact times and positions. Therefore, a low-cost, easy-to-use gait measurement system is required. Previously, we proposed gait measurement systems using a laser range sensor (LRS) (Matsumura, et al., 2013), (Yorozu and Takahashi, 2014). However, a system with a stationary LRS cannot be used for long-distance walking tests because its measurement range is limited by the detection range of the LRS.

To deal with these problems, we propose a novel gait measurement system which uses an autonomous mobile robot for a long-distance walking test in a real living space. Figure 2 shows an image of the proposed gait measurement robot. The robot sequentially estimates its own pose (localization) and acquires the position of both legs of the participant based on the distance data from the sensors. The robot leads the participant from the start to the goal of the walking test while maintaining a certain distance from the participant. Then, foot contact times and positions are calculated by analyzing the estimated position and speed of each leg. By maintaining a certain distance from the participant, the robot can make measurements for the long-distance walking test regardless of the detection range of the sensor. In addition, as shown in Figure 2, by leading the participant, the robot can provide instructions to the participant on how to make the movement, and we expect that the robot will also be able to evaluate not only motor function but also cognitive function of the participant from the response such as reaction time to the instructions.

In this paper, to verify the accuracy of the foot contact times and positions measured by the proposed robot, straight walking tests with young people were carried out. The foot contact times and positions acquired by the proposed system were compared with the result measured using a three-dimensional motion analysis system (VICON).

2 CONCEPTS

The proposed gait measurement robot sequentially process localization and acquires leg positions from sensor data and command speed determination to maintain a certain distance from the participant based on the estimated its own pose and leg positions. To define the field for the walking test and to estimate its own pose during the walking test, the

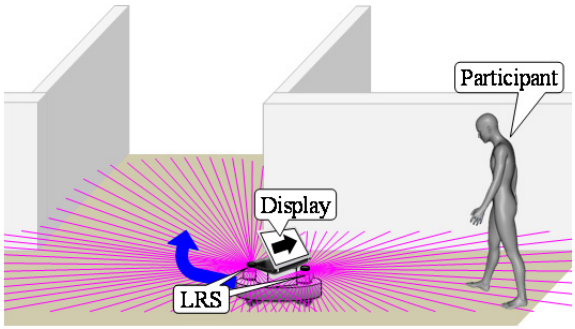

Figure 2: Image of the proposed gait measurement robot.

robot builds a map of the field based on simultaneous localization and mapping (SLAM) (Thrun, et al., 2005) before the walking test. In environment recognition during movement, it is desirable to be able to acquire high accuracy distance data over a wide range. With this in mind, LRSs are generally used in autonomous mobile robots. In addition, a method for calculating the leg positions based on the characteristic leg patterns from the LRS scan data has been proposed (Bellotto and Hu, 2009). A method to acquire the posture of the pedestrian based on the RGB data from a camera or RGB-Depth data from a KINECT has been proposed (Shotton, et al., 2011), (Ratsamee, et al., 2012). In this paper, because we intend to track both legs and measure the foot contact times and positions, LRSs that can obtain distance data over a wide range by a single unit are used to recognize the environment for localization and to acquire the leg positions. In future, when we need to measure other walking parameters, we will implement sensor fusion with other sensors to match the measurement items.

The robot is required a smooth movement according to the participant's motion. Additionaly, the robot is also required to move while facing the participant screen in order to give instructions to the participant. To realize such movement, an omnidirectional drive system that can control translational and rotational motion simultaneously is equiped and is designed to be able to put out an average of human walking speed.

Moreover, it has been reported that elderly people at high risk of falling tend to look close to their body (e.g., look at their feet) and find it difficult to recognize the surrounding environment during walking (Yamada, et al., 2012). To allow them to recognize the surrounding environment by keeping their gaze in front, the robot is designed to lead the participant while maintaining a 1.5 m distance from them.

3 GAIT MEASUREMENT ROBOT

3.1 System Configuration

Figure 3 shows the appearance of the proposed gait measurement robot. The robot is 0.26 m height, 0.40 m diameter and its weight is 11 kg. Two LRSs are equipped in front and back of the robot for recognition of the surrounding environment and gait measurement. Table 1 shows the specification of the LRS. In addition, the robot has an omnidirectional drive system composed by four wheels and the maximum speed of the robot is 2.5 m/s that is faster than the average of human walking speed (1.4 m/s). The wheel rotation data is able to be obtained by encoder.

Figure 4 shows the overview of the process of the gait measurement robot system. As shown in Figure 5, we define two coordinate systems. One is field coordinate system $\Sigma(x,y,\theta)$ and the other is robot coordinate system $\Sigma'(x',y',\theta')$, where the symbol dash indicates the robot coordinate.

As shown in Figure 4 (a), if the robot does not have a map of the walking test field, the robot builds a map by SLAM and determines the start and goal positions. In this study, the robot builds a two-dimensional occupancy grid map using the front LRS scan data.

In the gait measurement process shown in Figure 4 (b), the robot estimates its own pose in the field coordinate using the front LRS scan data and the map built in advance. In addition, the robot detects legs in the robot coordinate using the back LRS scan data and estimates the position and velocity of both legs in the field coordinate using the Kalman filter with the estimated own pose. Then, velocity command of the robot is successively determined with the artificial potential method based on the estimated robot pose and positions of the legs and the goal until the participant reaches the goal position. When the participant reaches the goal, the robot will stop and calculate the foot contact times and positions based on the acquired position and velocity of the legs.

3.2 Localization with Occupancy Grid Map

In the localization shown in Figure 4, the robot estimates its own pose based on the wheel rotation data of the encoders, LRS scan data and two-dimensional occupancy grid map. The occupancy grid map is capable of probabilistic representation and each cell has an existence probability of the object. $bel_k^{Map}(\mathbf{p})$ is the occupancy of the cell at the position $\mathbf{p}=[x \quad y]^T$. $bel_k^{Map}(\mathbf{p})$ is given depending

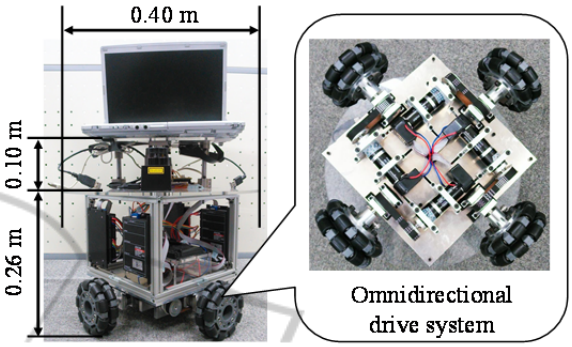

Figure 3: Appearance of the gait measurement robot.

Table 1: Specification of LRS (URG-04-LX-UG01, HOKUYO AUTOMATIC CO., LTD.).

Detection range	0.02 to 5.6 m, 240 deg
Accuracy	0.06 to 1.0 m: ± 0.03 m 1.0 to 4.0 m: ± 3% of measurement
Angular resolution	0.36 deg (360 deg/1024)
Scan time Δt	0.10 s/scan

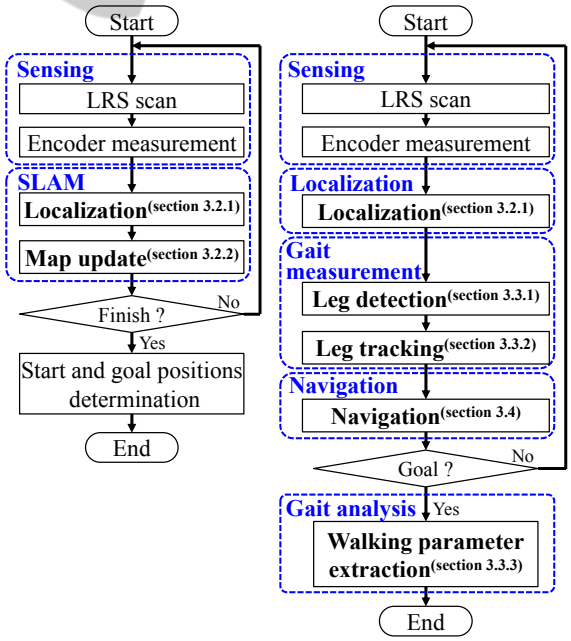

(a) Mapping (b) Gait measurement

Figure 4: Overview of the process of the gait measurement robot system.

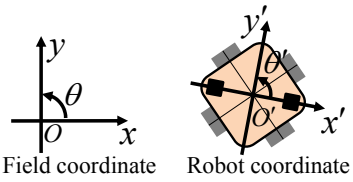

Figure 5: Coordinate systems of the robot and the field.

on the cell state as follows:

$$\begin{aligned} 0 < bel_k^{Map}(\mathbf{p}) \le 1 \quad & Occupied \\ -1 \le bel_k^{Map}(\mathbf{p}) < 0 \quad & Unoccupied \\ bel_k^{Map}(\mathbf{p}) = 0 \quad & Unknown \end{aligned} . \tag{1}$$

We set the cell size 0.03 m to estimate robot pose with a high accuracy.

3.2.1 Localization

As shown in Figure 4, the robot estimates its own pose using the sampling poses and those of likelihood calculated with the LRS scan data and the map in existence.

First, the sampling poses of the robot $\bar{\mathbf{p}}_k^{Robot}(\alpha,\beta,\gamma) = \begin{bmatrix} \bar{x}_k^{Robot} + \alpha\bar{x}_{th} \\ \bar{y}_k^{Robot} + \beta\bar{y}_{th} \\ \bar{\theta}_k^{Robot} + \gamma\bar{\theta}_{th} \end{bmatrix}$ at the time k are calculated based on the movement of the robot $\Delta\mathbf{p}'^{Enc}_{k-1} = \begin{bmatrix} \Delta x'^{Enc}_{k-1} & \Delta y'^{Enc}_{k-1} & \Delta\theta'^{Enc}_{k-1} \end{bmatrix}^T$ calculated from the wheel rotation data of encoders. $\bar{\mathbf{p}}_k^{Robot}(0,0,0) = \begin{bmatrix} \bar{x}_k^{Robot} & \bar{y}_k^{Robot} & \bar{\theta}_k^{Robot} \end{bmatrix}^T$ is a wheel odometry calculated as follows:

$$\begin{bmatrix} \bar{x}_k^{Robot} \\ \bar{y}_k^{Robot} \\ \bar{\theta}_k^{Robot} \end{bmatrix} = \begin{bmatrix} x_{k-1}^{Robot} \\ y_{k-1}^{Robot} \\ \theta_{k-1}^{Robot} \end{bmatrix} + \begin{bmatrix} \cos\left(\theta_{k-1}^{Robot}\right) & -\sin\left(\theta_{k-1}^{Robot}\right) & 0 \\ \sin\left(\theta_{k-1}^{Robot}\right) & \cos\left(\theta_{k-1}^{Robot}\right) & 0 \\ 0 & 0 & 1 \end{bmatrix} \begin{bmatrix} \Delta x'^{Enc}_{k-1} \\ \Delta y'^{Enc}_{k-1} \\ \Delta\theta'^{Enc}_{k-1} \end{bmatrix} \tag{2}$$

We set the parameters as $\alpha,\beta,\gamma = 0,\pm1,\pm2,\pm3$, $\bar{x}_{th}, \bar{y}_{th} = 0.03$ (= cell size) and $\bar{\theta}_{th} = \pi/60$.

Then, the likelihood $\mu(\alpha,\beta,\gamma)$ of the sampling pose $\bar{\mathbf{p}}_k^{Robot}(\alpha,\beta,\gamma)$ is calculated as follows:

$$\mu(\alpha,\beta,\gamma) = \frac{\sum_{n=1}^{N} bel_k^{Map}\left(\mathbf{p}_k^{l_n}(\alpha,\beta,\gamma)\right)}{N}, \tag{3}$$

where N is the number of LRS scan data which detects an object and $\mathbf{p}_k^{l_n}(\alpha,\beta,\gamma)$ is the position of the object detected by the n-th LRS scan data l_n in the field coordinate.

Finally, the estimated robot pose $\mathbf{p}_k^{Robot} = \begin{bmatrix} x_k^{Robot} & y_k^{Robot} & \theta_k^{Robot} \end{bmatrix}^T$ at the time k is determined as the sampling pose of maximum likelihood.

3.2.2 Map Update

In building a field map process shown in Figure 4 (a), the map is updated based on the probabilistic model of the LRS scan data and the estimated robot pose.

The object existence probabilistic model of the i-th LRS scan data from the center of the LRS to the object detection distance l_i is as follows (Yamaura, et al., 2005):

$$bel_k'^{l_i}(r) = \begin{cases} -1 + (r/l_i)^2 & 0 < r < l_i \\ 1 & r = l_i \\ 0 & else \end{cases}, \tag{4}$$

where r is the distance from the center of the LRS. Then, the occupancy of the cell at the position $\mathbf{p}$ is updated with the following equation:

$$bel_k^{Map}(\mathbf{p}) = bel_{k-1}^{Map}(\mathbf{p}) + \hat{\mu}\, bel_k^{LRS}(\mathbf{p}), \tag{5}$$

where $\hat{\mu}$ is the likelihood of the estimated robot pose and $bel_k^{LRS}(\mathbf{p})$ is the object existence probability of the LRS translated to the field coordinate considering the estimated robot pose.

3.3 Gait Measurement with LRS

As shown in Figure 4 (b), the robot detects legs in the robot coordinate using the back LRS scan data and estimates the position and velocity of both legs in the field coordinate using the Kalman filter with the estimated own pose. After the participant reaches the goal, the robot will stop and calculate the foot contact times and positions based on the acquired position and velocity of the legs.

3.3.1 Leg Detection

Leg positions at shin height are able to be calculated by the characteristic LRS scan data pattern (Bellotto and Hu, 2009). As shown in Figure 6, we classified

the legs into three leg patterns: LA (two Legs Apart), FS (Forward Straddle) and SL (Single Leg).

First, to detect the three leg patterns, the vertical edges shown in Figure 6 as a symbol " o " were extracted from LRS scan data using following equation:

$$|l_i - l_{i+1}| > 0.1 \ , \tag{6}$$

where l_i is the i-th scan data from the right of an LRS. Moreover, the detected edges are classified into two type: left edge when $l_i < l_{i+1}$ and right edge when $l_i > l_{i+1}$.

In classifying the legs into the three leg patterns, we define a, b and c which are, respectively the

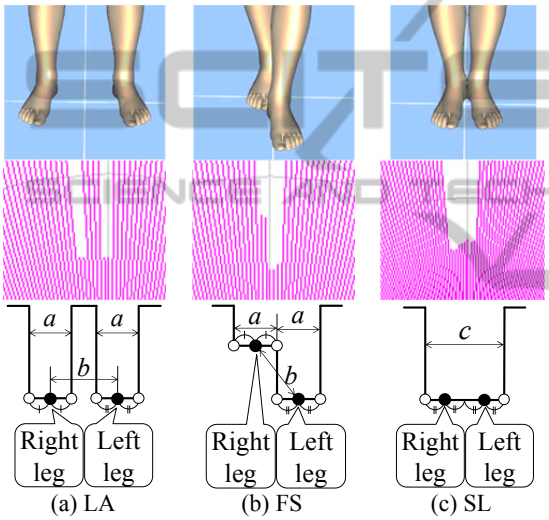

Figure 6: Leg patterns extracted from LRS scan data.

thresholds of, the leg width, the maximum step length and the width of the two legs together. Then, the leg pattern was detected by using three leg parameters and the combination of the arrangement of the edges. We set these thresholds as $0.01 < a < 0.20$, $0.10 < b < 1.0$ and $0.20 < c < 0.40$. Finally, left and right leg positions in the robot coordinate shown in Figure 6 as a symbol "•" are calculated based on the leg patterns.

3.3.2 Leg Tracking with Kalman Filter

There are noise of the observed leg positions and the localization error. Therefore, the robot estimates the leg position and velocity in the field coordinate using Kalman filter with the observed leg position in the robot coordinate and estimated the robot pose in the field coordinate (Kakinuma, et al., 2011).

If the sampling time Δt (0.10 s in our robot) is sufficiently shorter than the gait cycle time, the discrete time model of leg motion is as follows:

$$\mathbf{x}_k^f = \mathbf{A}\mathbf{x}_{k-1}^f + \mathbf{B}\Delta\mathbf{x}_{k-1}^f \ (f = L, R), \tag{7}$$

where $\mathbf{A} = \begin{bmatrix} 1 & 0 & \Delta t & 0 \\ 0 & 1 & 0 & \Delta t \\ 0 & 0 & 1 & 0 \\ 0 & 0 & 0 & 1 \end{bmatrix}$, $\mathbf{B} = \begin{bmatrix} \Delta t^2/2 & 0 \\ 0 & \Delta t^2/2 \\ \Delta t & 0 \\ 0 & \Delta t \end{bmatrix}$,

and $\mathbf{x}_k^f = \begin{bmatrix} x_k^f & y_k^f & \dot{x}_k^f & \dot{y}_k^f \end{bmatrix}^T$. $\left(x_k^f, y_k^f\right) := \mathbf{p}_k^f$ is the estimated position and $\left(\dot{x}_k^f, \dot{y}_k^f\right) := \mathbf{v}_k^f$ is the estimated velocity of the leg in the field coordinate ($f = L, R$ indicates the Left and Right leg respectively). $\Delta\mathbf{x}_k^f = \begin{bmatrix} n^{\dot{x}_k} & n^{\dot{y}_k} \end{bmatrix}^T$ is the acceleration

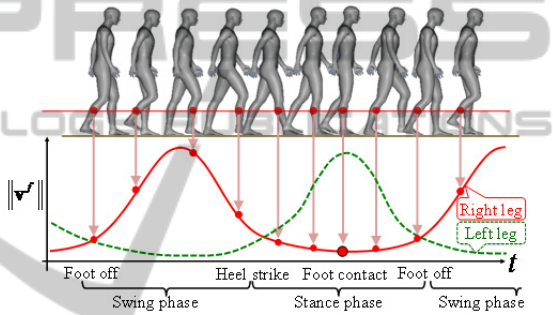

Figure 7: Gait speed diagram during walking.

disturbance vector, which is assumed to be zero mean and has a white noise sequence with variance $\mathbf{Q}$. In experiments, we set the variance as $\mathbf{Q} = \mathrm{diag}\left[(1.4)^2, (1.4)^2\right]$. The leg position $\mathbf{y}_k'^f = \begin{bmatrix} x_k'^f & y_k'^f \end{bmatrix}^T$ in the robot coordinate is given from the leg detection. The measurement model is defined using the estimated robot position $\mathbf{y}_k^{Robot} = \begin{bmatrix} x_k^{Robot} & y_k^{Robot} \end{bmatrix}^T$ at the time k in the field coordinate as follows:

$$\mathbf{y}_k'^f = \mathbf{C}\mathbf{x}_k^f + \mathbf{C}'\mathbf{y}_k^{Robot} + \Delta\mathbf{y}_k'^f, \tag{8}$$

where $\mathbf{C} = \begin{bmatrix} \cos\theta_k^{Robot} & \sin\theta_k^{Robot} & 0 & 0 \\ -\sin\theta_k^{Robot} & \cos\theta_k^{Robot} & 0 & 0 \end{bmatrix}$ and

$\mathbf{C}' = \begin{bmatrix} -\cos\theta_k^{Robot} & -\sin\theta_k^{Robot} \\ \sin\theta_k^{Robot} & -\cos\theta_k^{Robot} \end{bmatrix}$. θ_k^{Robot} is also the estimated yaw angle of the robot at the time k. $\Delta\mathbf{y}_k'^f = \begin{bmatrix} n^{x_k'} & n^{y_k'} \end{bmatrix}^T$ is the measurement noise, which is assumed to be zero mean and has a white

noise sequence with variance $\mathbf{R}$. In our experiments, we set the variance as $\mathbf{R} = \mathrm{diag}\left[(0.03)^2, (0.03)^2\right]$ considering the measurement accuracy of the LRS.

3.3.3 Walking Parameter Extraction

After the participant reaches the goal shown in Figure 4 (b), the robot will stop and calculate the foot contact times and positions based on the acquired position and velocity of the legs.

In this study, we define the foot contact time as the foot bottom is attached to the floor and the leg is perpendicular to the floor. As shown in Figure 7, the speed of the leg at shin height scaned by LRS is minimum value at the time. Therefore, the foot contact time is extracted as the time when the leg speed is at a minimum value. In addition, the foot contact position is acquired as the estimated position at that time.

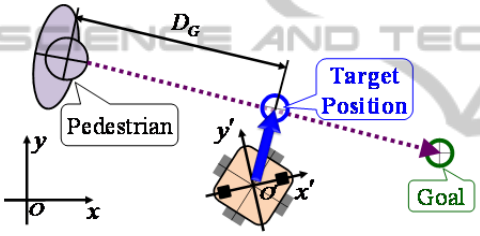

Figure 8: Design of the attractive potential to lead the participant while maintaining a certain distance. D_G

3.4 Navigation based on Artificial Potential Method

In order to realize that the robot leads the participant to the goal position, the velocity command is determined based on the artificial potential method (Khatib, 1986).

In the potential method, the potential field is designed with an attractive potential field based on the goal position and repulsive potential field based on the obstacle position. Then, the robot determines the motion based on the vertical force derived from the potential field.

As shown in Figure 8, to lead the participant while maintaining the certain distance D_G from the participant, the target position of the robot is defined as the position which is D_G distance to the goal direction from the participant. Then, the attractive potential is designed based on the target position. To allow the participant to recognize the surrounding environment by keeping their gaze in front, we set $D_G = 1.5$. Determination of the velocity command considering the velocity of the participant is future work.

4 EXPERIMENT

To verify the accuracy of the foot contact times and positions measured by the proposed gait measurement robot, we carried out straight walking test with five young people. The foot contact times and positions measured by the proposed robot compared with those measured by the three-dimensional motion analysis system (VICON) with six cameras. Figure 9 shows the field of the straight walking test. As shown in Figure 10, the robot built the environmental map in advance. The cell size was set to 0.03 m. In addition, the field coordinate system of the proposed system was fixed to that of VICON by using poles shown in Figure 9.

As shown in Figure 11, VICON markers were attached to the 18 places in the lower limbs of the participant and Plug-In-Gait model was used for motion analysis. In addition, for verification of the trajectory of the legs, additional markers were attached to each leg at the same height of the LRS. Furthermore, for verification of the robot localization, markers were attached to the front and back of the robot shown in Figure 11. The true pose of the robot was calculated using the two markers.

In this study, we define the foot contact time as the foot bottom is attached to the floor and the leg is perpendicular to the floor. From the VICON analysis,

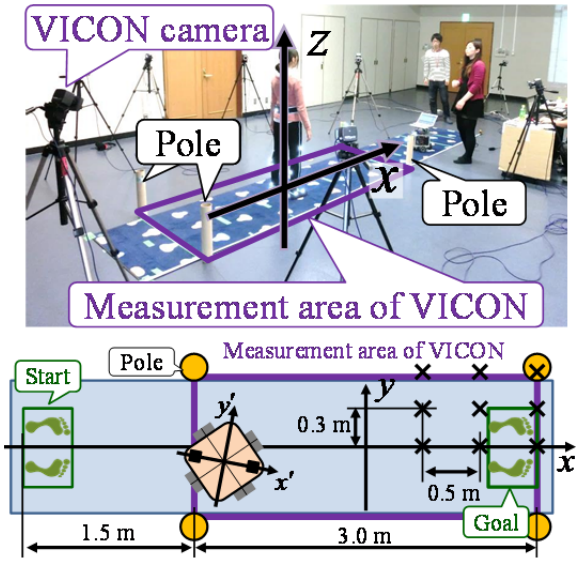

Figure 9: Experimental field.

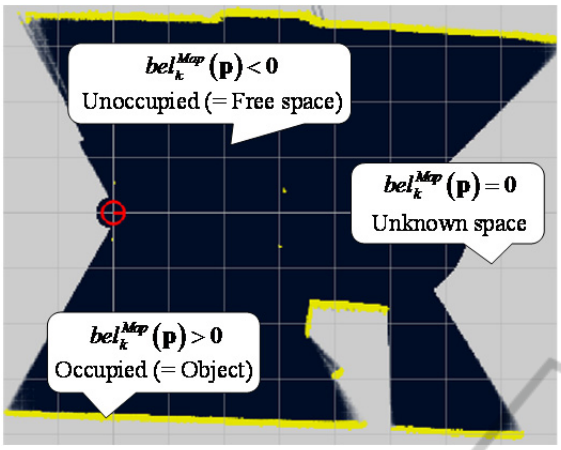

Figure 10: Map built by the robot in the experimental field.

Figure 11: Positions of the attached VICON markers.

Table 2: Acquired leg position error (*x*-coordinate).

Position		Mean [m]			SD [m]		
		x					
		0.5	1.0	1.5	0.5	1.0	1.5
y	0.0	0.017	0.016	0.013	0.010	0.013	0.011
	0.3	0.015	0.014	0.010	0.010	0.010	0.008
	0.6	0.009	0.022	0.019	0.008	0.011	0.011

Table 3: Acquired Leg position error (*y*-coordinate).

Position		Mean [m]			SD [m]		
		x					
		0.5	1.0	1.5	0.5	1.0	1.5
y	0.0	0.022	0.031	0.035	0.026	0.029	0.030
	0.3	0.020	0.023	0.027	0.027	0.026	0.026
	0.6	0.028	0.023	0.024	0.023	0.023	0.024

it was confirmed that the time when the marker of the heel was not moving was almost equal to the time when the leg was perpendicular to the floor. Therefore, the true value of the foot contact time was calculated as the time when the speed of the heel marker was at a minimum. Then, the foot contact position was acquired as the position of the heel marker at that time. As shown in Figure 11, since the measurement points of the robot were different those of VICON, the positions of the legs acquired by the robot were modified considering the leg width of the participant to compare with the VICON analysis.

4.1 Verification in Stationary State

We verified the accuracy of the localization and the leg positions acquired by the robot in stationary state.

4.1.1 Localization

The robot stayed at nine points shown in Figure 9 as a symbol "×". The accuracy of localization for 5.0 s in each point was verified. The maximum localization errors of *x*-coordinate, *y*-coordinate and yaw angle were respectively 0.070 m, 0.020 m and 0.030 rad. It was confirmed that the proposed robot was able to estimate its own pose with high accuracy equivalent to that of the measurement accuracy of the LRS.

4.1.2 Leg Position

The robot stayed at the origin of the field and the participant was standing at nine points shown in Figure 9 as a symbol "×". The accuracy of the acquired leg position of each point for 5.0 s was verified. Table 2 and 3 show the mean and the standard deviation (SD) of the measurement error of the right leg position acquired by the robot compared with the heal position acquired by VICON in each point. From the results in stationary state, it was confirmed that the proposed robot could measure the foot position with high accuracy equivalent to that of the measurement accuracy of the LRS.

4.2 Verification in Straight Walking Test

We verified the accuracy of the localization and acquired foot contact times and positions in straight walking test.

4.2.1 Localization

Figure 12 show an example of the results of localization in straight walking test. The mean of the localization error of *x*-coordinate, *y*-coordinate and yaw angle were respectively 0.043 m, 0.036 m and 0.020 rad. It was confirmed that the proposed robot was able to estimate its own pose in moving state with the same accuracy in stationary state.

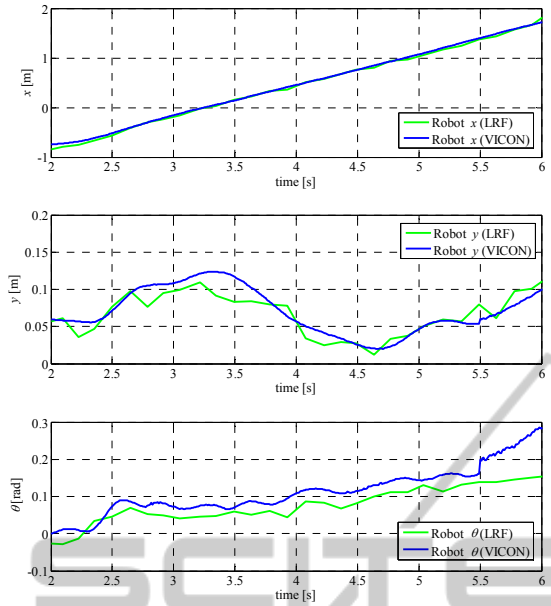

(a) Localization

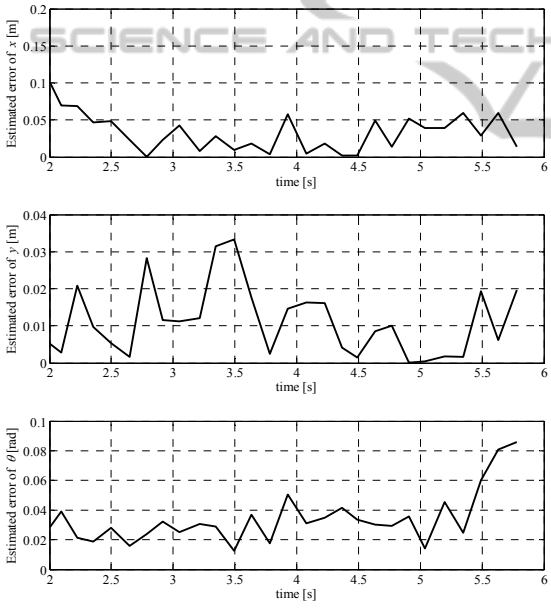

(b) Localization error

Figure 12: An example of the results of localization in straight walking test.

4.2.2 Foot Contact Time

Figure 13 shows the an example of the results of the speed of the right leg acquired by the proposed robot and the speed of the calf positions aquired by VICON. The mean and SD of the error of the foot contact time in five walking test were 0.147 s and 0.110 s. From the results, it was comfirmed that the proposed robot could acquire the foot contact time based on the estimated speed of the leg.

4.2.3 Foot Contact Position

Figure 14 shows an example the results of right leg position and foot contact positions acqurired by the proposed robot and the heel and calf positions acquired by VICON. The total measurement error mean and SD of the foot contact positions of *x*-coordinate were 0.035 m, 0.031 m and the those of *y*-coordinate were 0.036 m, 0.023 m. From the experimental results, it was comfirmed that the proposed robot can acquire the foot contact positions while leading the participant to the goal position of the walking test field.

5 CONCLUSIONS

In this study, we proposed a novel gait measurement system which uses an autonomous mobile robot with laser range sensor (LRS) for a long-distance walking test in a real living space regardless of detection range of sensor. To realize smooth movement depending on the movement of the participant, the robot has an omnidirectional drive system and is

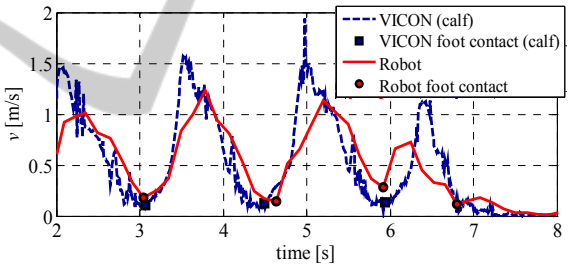

Figure 13: An example of the results of acquired leg speed and foot contact time.

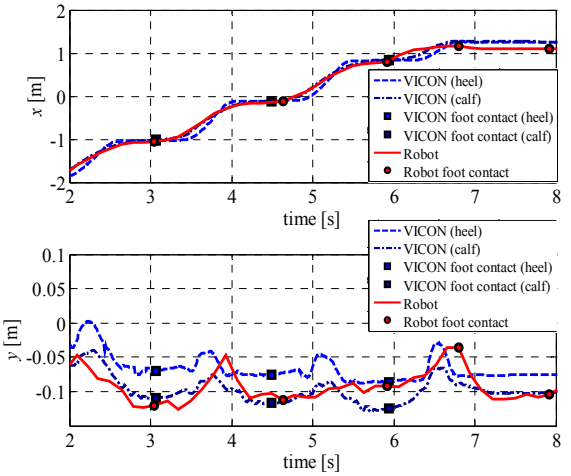

Figure 14: An example of the results of acquired right leg position and foot contact position.

designed to be able to put out an average of human walking speed. The robot sequentially estimates its own pose and acquires both legs of the participant based on the distance data from the sensors. The robot leads the participant from the start to the goal of the walking test while maintaining a certain distance from the participant. Then, the foot contact times and positions are calculated by analyzing estimated position and speed of each leg.

To verify the accuracy of the foot contact times and positions acquired by the proposed robot, straight walking test with five young people were carried out. From the experimental results compared with a three-dimensional motion analysis system (VICON), it was confirmed that the proposed robot could acquire the foot contact times and positions.

Experiments with elderly people in living space and verifications for the characteristic motion such as cross step where the participant cross the swinging leg against the supporting leg are future work. In addition, velification of the robustness of the localization of the robot in a real living space and leg tracking is future work.

ACKNOWLEDGEMENTS

This work was supported by Grant-in-Aid for Japan Society for the Promotion of Science (JSPS) Fellows Grant Number 25-5707 and JSPS KAKENHI Grant Number 25709015.

REFERENCES

Bellotto, N., Hu, H., 2009. Multisensor-Based Human Detection and Tracking for Mobile Service Robots, *IEEE Transactions on Systems, Man and Cybernetics-Part B: Cybernetics*, Vol. 39, No. 1, pp. 167-181.

Davis, R., Õunpuu, S., Tyburski, D., Gage, J., 1991. A gait analysis data collection and reduction technique, *Journal of Human Movement Scienc*, Vol. 10, No. 5, pp. 575-587.

HOKUYO AUTOMATIC CO, LTD., available from <http://www.hokuyo-aut.jp/>, (accessed on 24 June, 2014).

Kakamigahara Health Promotion Power-up Business "Lively Health Challenge 2007 spring", available from <http://www.waseda.jp/prj-i4id/kakamigahara/project/event/070519/02.html>, (accessed on 24 June, 2014), (in Japanese).

Kakinuma, K., Ozaki, M., Hashimoto, M., Yokoyama, T., Takahashi, K., 2011. Laser-Based Pedestrian Tracking with Multiple Mobile Robots Using Outdoor SLAM, *IEEE International Conference on Robotics and Biomimetics 2011*, pp. 998-1003.

Khatib, O., 1986. Real-time Obstacle Avoidance for Manipulators and Mobile Robots, *International Journal of Robotics Research*, Vol. 5, No. 1, pp. 90-98.

Matsumura, T., Moriguchi, T., Yamada, M., Uemura, K., Nishiguchi, S., Aoyama, T., Takahashi, M., 2013. Development of measurement system for task oriented step tracking using laser range finder. *Journal of NeuroEngineering and Rehabilitation*, Vol. 10, No. 47.

Melzer, I., Oddsson, L., 2004. The effect of a cognitive task on voluntary step execution in healthy elderly and young individuals, *Journal of the American Geriatrics Society*, Vol. 52, pp. 1255-1262.

Melzer, I., Shtilman, I., Rosenblatt, N., Oddsson, L., 2007. Reliability of voluntary step execution behavior under single and dual task conditions, *Journal of NeuroEngineering and Rehabilitation*, Vol. 4.

Ratsamee, P., Mae, Y., Ohara, K., Takubo, T., Arai, T., 2012. People Tracking with Body Pose Estimation for Human Path Prediction, *IEEE International Conference on Mechatronics and Automation 2012*, pp. 1915-1920.

Schoene, D., Load, S.R., Delbaere, K., Severino, C., Davies, T.A., Smith, S.T., 2013. A Randomized Controlled Pilot Study of Home-Based Step Training in Older People Using Videogame Technology, *Journal of PLOS ONE*, Vol. 8.

Shotton, J., Fitzgibbon, A., Cook, M., Sharp, T., Finocchino, M., Moore, R., Kipman, A., Blake, A., 2011. Real-time Human Pose Recognition in Parts from Single Depth Images, *CVPR*.

Tinetti, M.E., Speechley, M., Ginter, S.E., 1988. Risk factors for falls among elderly persons living in the community, *New England Journal of Medicine*, Vol. 319, pp.1701-1707.

Thrun, S., Burgard, W., Fox, D., 2005, Probabilistic Robotics, *MIT press*.

World Health Organization, 2008. WHO Global Report on Falls Prevention in Older Age, *WHO press*.

Yamada, M., Tanaka, B., Nagai, K., Aoyama, T., Ichihashi, N., 2011. Rhythmic stepping exercise under cognitive conditions improves fall risk factors in community-dwelling older adults: Preliminary results of a cluster-randomized controlled trial, *Aging & mental health*, Vol. 15, pp.647-653.

Yamada, M., Higuchi, T., Mori, S., Uemura, K., Nagai, K., Aoyama, T., Ichihashi, N., 2012. Maladaptive turning and gaze behavior induces impaired stepping on multiple footfall targets during gait in older individuals who are at high risk of falling, *The Archives of Gerontology and Geriatrics*, Vol. 54, pp. 102-108.

Yamaura, K., Kamata, N., Taira, T., Yamasaki, N., 2005. A Map Generation System by using Movable Infrared Sensors for an Autonomous Mobile Robot, *ROBOMEC2005*, (in Japanese).

Yorozu, A., Takahashi, M., 2014. Gait Measurement System for the Elderly Using Laser Range Sensor, *Applied Mechanics and Materials*, Vols. 490-491, pp. 1629-1635.